Low-Dimensional Photocatalysts for CO2 Conversion

Subjects: Materials Science, Characterization & Testing

Contributor: Hyeonseok Lee

The ongoing energy crisis and global warming caused by the massive usage of fossil fuels and emission of CO2 into atmosphere continue to motivate researchers to investigate possible solutions. The conversion of CO2 into value-added solar fuels by photocatalysts has been suggested as an intriguing solution to simultaneously mitigate global warming and provide a source of energy in an environmentally friendly manner. There has been considerable effort for nearly four decades investigating the performance of CO2 conversion by photocatalysts, much of which has focused on structure or materials modification. In particular, the application of low-dimensional structures for photocatalysts is a promising pathway. Depending on the materials and fabrication methods, low-dimensional nanomaterials can be formed in zero dimensional structures such as quantum dots, one-dimensional structures such as nanowires, nanotubes, nanobelts, and nanorods, and two-dimensional structures such as nanosheets and thin films. These nanostructures increase the effective surface area and possess unique electrical and optical properties, including the quantum confinement effect in semiconductors or the localized surface plasmon resonance effect in noble metals at the nanoscale.

photocatalysis carbon dioxide conversion nanostructures low-dimensional photocatalysts

solar fuels

1. Background

The fast-developing modern technology and explosive world population growth have resulted in a huge demand for and consumption of energy. According to an investigation from the U.S. Energy Information Administration, more than 600 quadrillion Btus of energy were spent in 2020 and it is expected that the demand will continue to skyrocket annually. To meet this huge energy demand every year, energy production has been predominately dependent on fossil fuels such as coal, oil, or natural gas. The energy production by fossil fuels is inextricably linked to the gigantic CO_2 emission of more than 30 billion metric tons every year and, in turn, the accumulated CO_2 in our atmosphere is deemed to be the main cause of many environmental problems such as global warming and erratic weather patterns. In this context, there is great motivation to find a way of reducing atmospheric CO_2 and producing energy at the same time. For these problems, CO_2 conversion by photocatalyst materials under light illumination could be an expedient solution. This is because natural sunlight provides clean, renewable, and abundant energy, and photocatalysts can be activated by light energy from the Sun, while simultaneously consuming CO_2 for energy production.

In 1978, by Halmann [1], the first demonstration of the photocatalytic conversion of CO_2 in aqueous solution into liquid fuels such as methanol, formic acid, and formaldehyde was achieved over p-type gallium phosphide semiconductor. The same year, the photoartificial synthesis by $SrTiO_3$ photocatalysts for CH_4 production through the gas-solid phase reaction of CO_2 and H_2O was reported by Hemminger [2]. In 1979, another pioneering work by Fujishima and his coworkers introduced the artificial synthesis of solar fuels from a CO_2-saturated electrolyte under light illumination. In this study, liquid CO_2 was converted with various semiconductor photocatalysts such as TiO_2, ZnO, CdS, GaP, SiC, and WO_3 to produce methane, methanol, formaldehyde and formic acid [3]. Since these historical works mentioned above, several semiconductor materials have been investigated for the conversion of CO_2 into useful fuels, including graphitic carbon nitride (g-C_3N_4), graphene, conjugated polymers, covalent organic framework, metal organic frameworks, metal chalcogenides, metal oxides, black phosphorus, bismuth-based materials, and perovskites [4][5][6][7][8][9][10][11][12][13][14]. Moreover, a variety of strategies and approaches have been applied to improve the photocatalyst performance through elemental doping, solid solution, heterostructure, nanostrucutralization, surface engineering and modification, crystal facet engineering, cocatalysts utilization, or dimensionality tailoring [15][16][17][18][19].

Of the strategies researched to boost the efficiency of CO_2 conversion, decreasing the dimensionality and constructing nanostructures of the photocatalyst have attracted a lot of attention owing to their favorable advantages in photocatalysis: first, nanostructured photocatalysts suppress the carrier recombination due to their higher crystallinity compared to non-nanostructured materials [20][21][22]; second, the implementation of low dimensionality modifies the electronic structure of bulk materials due to the quantum confinement effect in semiconductors or localized surface plasmon resonance effect in noble metals at the nanoscale; third, low-dimensional materials possess larger surface-area-to-volume ratio in comparison with bulk materials, providing more reaction sites. All three features can contribute to improved solar-driven catalytic reactions [19][23].

2. The Main Fundamentals of CO_2 Photoconversion into Solar Fuels and Hydrocarbon Species

2.1. Nature of CO_2

Carbon dioxide (CO_2) is one of the primary greenhouse gases but, at the same time, it is the main resource for solar fuel production when coupled with proton donors such as H_2O for photocatalytic CO_2 conversion. Hence, understanding the nature of the gaseous CO_2 molecule itself is necessary for efficient utilization of photocatalysts. CO_2 is a stable linear molecule among carbon compounds because of it is in the highest oxidation state of carbon, C^{+4} [19]. The CO_2 molecule has two C=O bonds with a dissociation energy of ~750 kJ/mol, which is quite larger than those in other chemical bonds such as C-H (~430 kJ/mol) and C-C (~336 kJ/mol). For this reason, the reduction of CO_2 to produce solar fuels requires additional energy to break the C=O bond and form, for example, a C-H bond [24]. Owing to its stability and strong bonding, photocatalytic reduction of CO_2 into solar fuels can be achieved primarily with the support of proton donors such as H_2O or H_2 [25].

2.2. CO_2 Adsorption on the Surface of Photocatalysts

The adsorption and activation of CO_2 on a solid surface is one of the essential steps in achieving CO_2 reduction and photocatalytic performance. The adsorption mechanism of CO_2 on several semiconductor photocatalysts has been investigated [26][27]. For instance, the adsorption of CO_2 on TiO_2 surface has been investigated by Minot and coworkers [26]. Various adsorption modes of CO_2 over a rutile TiO_2 surface have been studied using first-principles calculations. The oxygen atom of CO_2 molecules favors the interaction with the acidic titanium cation over the surface forming a Ti–OCO bond [26]. The adsorption of CO_2 on a photocatalyst surface includes the interaction between the CO_2 molecule and the surface atoms of the photocatalyst. This absorption may occur with a charge transfer from the photocatalyst to the linear and stable CO_2 molecule which can induce the formation of partially charged and bent adsorbate, COδ·−2, and this adsorbate can form three different molecular structures, as shown in Figure 1: oxygen coordination, carbon coordination, and mixed coordination [24][28][29]. The beneficial feature of COδ·−2, is that it has decrease in the lowest unoccupied molecular orbital (LUMO) of the CO_2 energy level as linear CO_2 molecule transformed into the bent structure. This would facilitate the charge transfer between a photocatalyst and COδ·−2, [24][28][29].

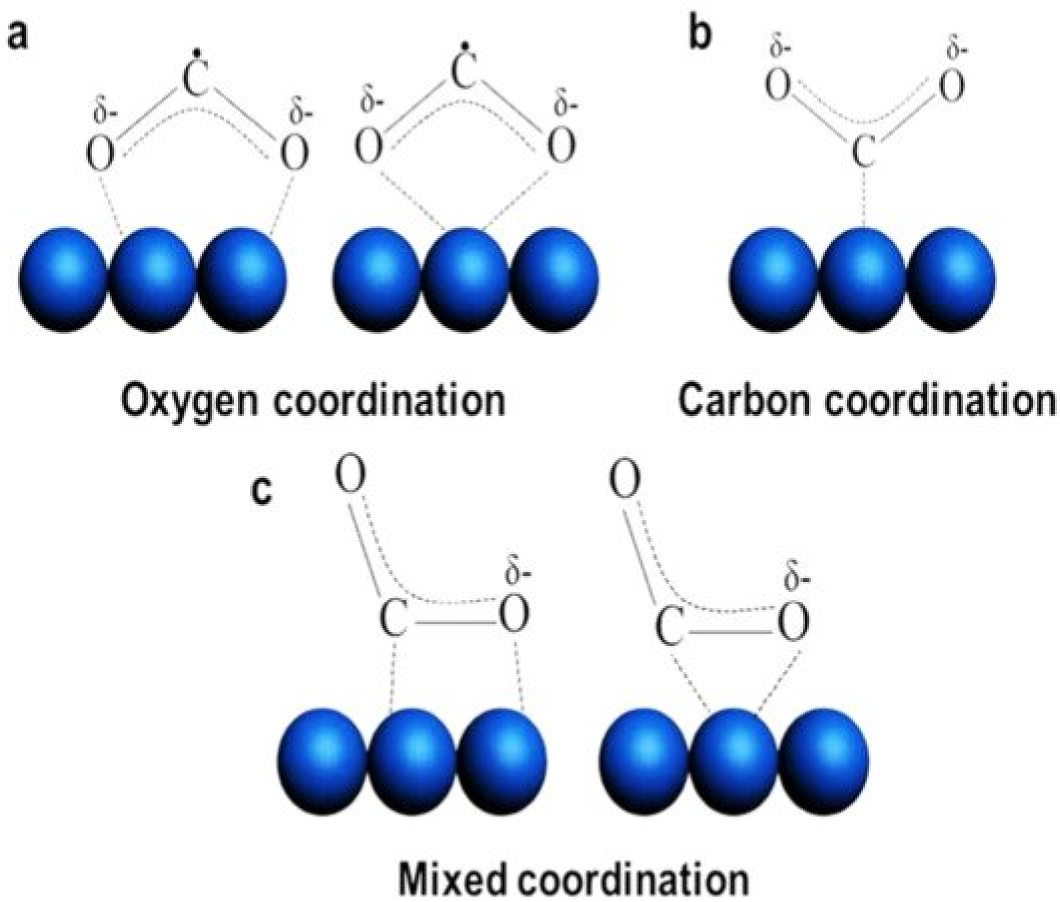

Figure 1. Schematic illustration of the different types of CO_2 adsorption modes (Adapted from [24]).

In the photocatalytic reaction, the photocatalyst donates electron to the adsorbed species on the surface to initiate the reduction process of CO_2 in the presence of protons. As shown in Table 1, the solar fuel production is determined by the number of electrons and protons included in the reaction [20][24]. For example, two electrons are required for CO evolution, while methane production is an eight-electron reaction. The adsorption of CO_2 on the photocatalyst surface can be improved by a variety of strategies. First, decreasing the structural dimensionality of photocatalyst can improve the surface area of the photocatalyst to allow more adsorption. Second, enhanced density of active sites by incorporation of surface defects, such as oxygen and sulfur vacancies, can improve the CO_2 adsorption. Third, utilization of noble metal nanoparticles can help improve the adsorption due to lowered activation energy of the CO_2 reduction [24][30].

Table 1. Standard electrochemical potentials of CO_2 and H_2O at 25 °C and atmospheric pressure [20][24].

Reaction	E^o at pH 7 (V vs. NHE)	Solar Fuel	
CO_2 reduction	$CO_2 + 2H^+ + 2e^- \rightarrow CO + H_2O$	−0.51	CO
	$CO_2 + 8H^+ + 8e^- \rightarrow CH_4 + 2H_2O$	−0.24	CH_4
	$CO_2 + 6H^+ + 6e^- \rightarrow CH_3OH + H_2O$	−0.39	CH_3OH
	$2CO_2 + 12H^+ + 12e^- \rightarrow C_2H_5OH + 3H_2O$	−0.33	C_2H_5OH
	$CO_2 + 2H^+ + 2e^- \rightarrow HCOOH$	−0.58	HCOOH
	$CO_2 + 4H^+ + 4e^- \rightarrow HCHO + H_2O$	−0.48	HCHO
H_2O oxidation	$2H_2O \rightarrow O_2 + 4H^+$	+0.81	O_2

2.3. The Mechanism of Efficient CO_2 Photoconversion

Upon absorption of light over the photocatalyst, charge carrier pairs are generated to achieve the photosynthesis of solar fuels accompanying the water splitting as shown in Table 1. To execute the conversion of CO_2 into useful fuels from the thermodynamic point of view, the conduction band minimum (CBM), and the valence band maximum (VBM) of a photocatalyst should bracket the redox potential of CO_2 and the oxidation potential of water, respectively, as shown in Table 1 and Figure 2. As results of the reactions, various solar fuels can be formed dependent on the number of electrons and protons in the presence of CO_2 and water under the illumination.

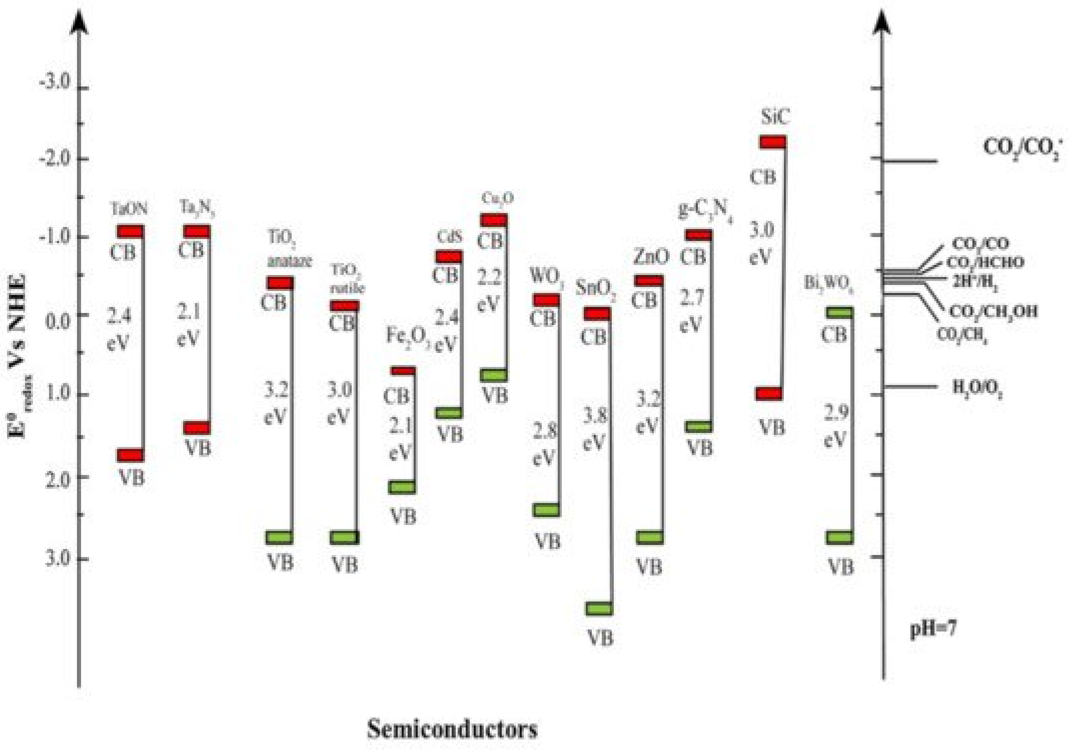

Figure 2. The energy band structures of semiconductor photocatalysts and the corresponding redox potentials of CO_2 reduction into solar fuels (Adapted from [31]).

The artificial photosynthesis of solar fuels using semiconductor photocatalysts consists of three essential steps, as described in Figure 3. Firstly, incident photons of light with energy higher than that of semiconductor band gap (E_g) induce the generation of the electron-hole pairs (Process (i)). Secondly, the photogenerated charge carriers are transferred to the photocatalyst surface (Process (ii)). Thirdly, the electrons and holes react on the surface of photocatalyst with CO_2 and H_2O for evolution of solar fuels (Process (iii)). For efficient photocatalytic conversion of CO_2 into fuels, the ideal semiconductor photocatalyst should have optimized band gap for efficient light harvesting and photocarrier generation, facile charge separation and transportation, vigorously activated sites and high surface area for maximum adsorption of CO_2 and water [30][32].

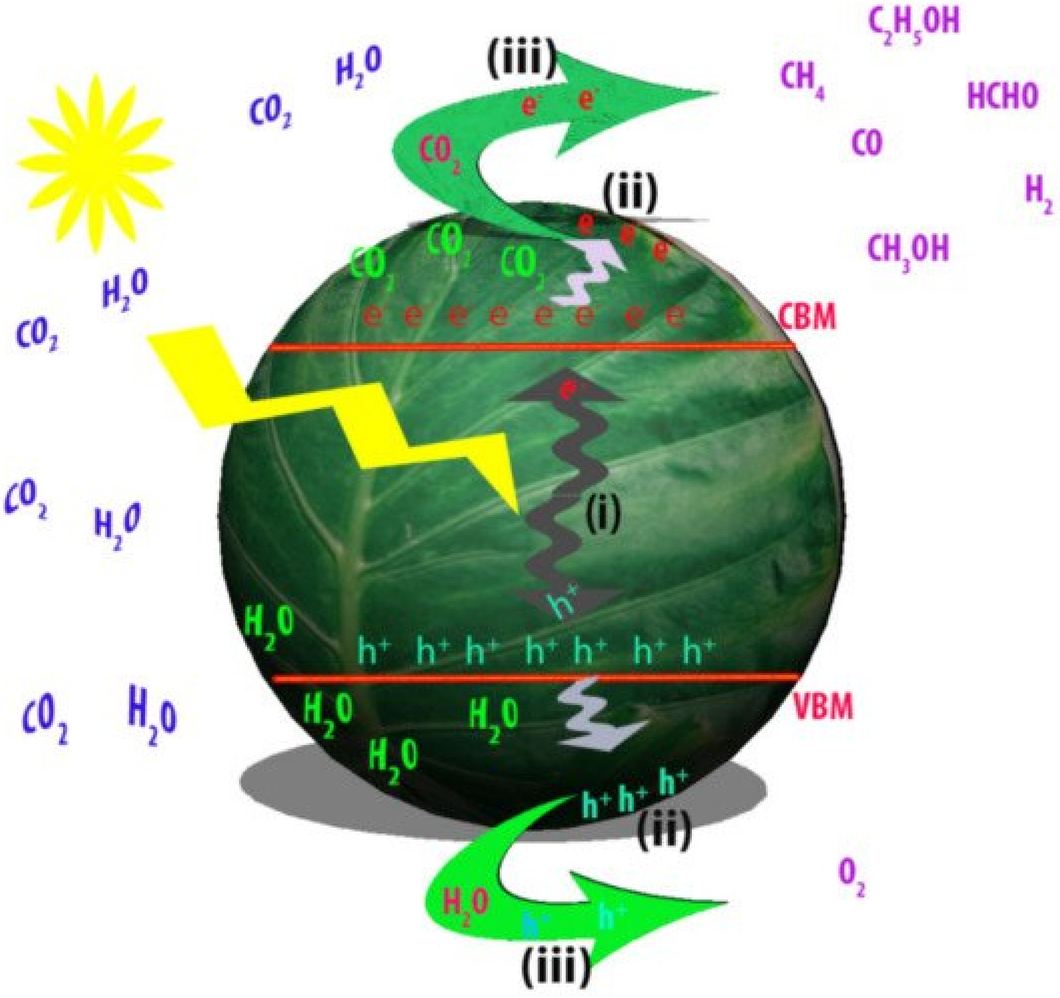

Figure 3. A schematic diagram of CO_2 photocatalytic conversion process over photocatalyst. Process (**i**): light absorption and generation of photocarriers via a semiconductor photocatalyst. Process (**ii**): charge carrier separation and transfer to the surface of photocatalyst. Process (**iii**): reactions of CO_2 and H_2O with electrons and holes, respectively to produce solar fuels.

3. Strategies for Enhancement in the Light-Driven CO_2 Conversion over Low-Dimensional Photocatalysts

Applying low-dimensional structure to the photocatalytic system itself is a proven way for obtaining high CO_2 conversion performance. However, further improvement is available by designing the structures or modifying the photocatalytic materials so that characteristics of photocatalysts or photocatalytic system are engineered. Here, we focus on these two major strategies for further enhancement of CO_2 conversion by low-dimensional photocatalysts. Table 2 summarizes the examples mentioned in this section.

Table 2. Summary of low-dimensional photocatalysts used in photocatalytic reduction of CO_2 into solar fuels. NC: Nanocrystal, GQD: Graphene Quantum Dot, NF: Nanofiber, NS: Nanosheet, CNT: carbon nanotube, Mt: montmorillonite, m-CN: modified g-C_3N_4, NR: nanorod, NW: nanowire, CND: carbon nano dot, p-CN: protonated g-

C_3N_4, PGCN: porous g-C_3N_4, TEOA: triethanolamine, bpy: bipyridine, C_3N_4: Melon-based polymeric carbon nitride, UTNS: ultrathin nanosheet, P-g-C_3N_4: Phosphorus doped g-C_3N_4.

Dimensionality	Morphology	Photocatalyst	Light Source	Reducing Agent	Main Product	Activity [μmol·g^{-1}·h^{-1}]	Ref.
0D	QD 3–12 nm	$CsPbBr_3$	300 W Xe lamp	H_2O	CO CH_4	4.26 1.53	[33]
	QD 2.3 nm	$Cs_3Bi_2I_9$	300 W Xe lamp	H_2O	CO	1.15	[34]
	QD 2.9 nm	$Cs_3Bi_2Br_9$	300 W Xe lamp	H_2O	CO	26.95	
	QD 2.4 nm	$Cs_3Bi_2Cl_9$	300 W Xe lamp	H_2O	CO	21.01	
	NC 9.5 nm	$Cs_2AgBiBr_6$	AM 1.5G	Ethyl acetate	CO CH_4	2.35 1.6	[35]
	QD 9.45 nm	$FAPbBr_3$	300 W Xe arc lamp	H_2O	CO CH_4	181.25 16.9	[36]
	QD 5.86 nm	GQD	300 W Xe lamp 420 nm cutoff filter	H_2O	CH_3OH	0.695	[11]
1D	NR	CeO_2	300 W Xe lamp	H_2O	CO	0.020	[37]
	NT	TiO_2	300 W Xe arc lamp 320 nm < λ < 780 nm	H_2O	CH_4	2.128	[21]
	NR	TiO_2	300 W Xe arc lamp 320 nm < λ < 780 nm	H_2O	CH_4	1.41	[21]
	NT	P-g-C_3N_4	300 W Xe lamp	H_2O/TEOA	CO CH_4	2.37 1.81	[38]

Dimensionality	Morphology	Photocatalyst	Light Source	Reducing Agent	Main Product	Activity [μmol·g^{-1}·h^{-1}]	Ref.
	NT	PGCN	300 W Xe lamp	H_2O/MeCN /TEOA	CO	103.6	[39]
	NT	$Bi_{12}O_{17}Cl_2$	300 W Xe lamp	H_2O	CO	48.6	[40]
	NT	$Bi_{12}O_{17}Br_2$	300 W Xe lamp	H_2O	CO	34.5	[41]
2D	NS	g-C_3N_4	300 W Xe arc lamp	MeCN/TEOA (4:1)	CO CH_4	5.407 1.549	[42]
	UTNS	g-C_3N_4	300 W Xe lamp	H_2O	CH_4 CH_3OH	1.39 1.87	[43]
	UTNS	SiC	300 W Xe lamp	H_2O	CO CH_4	1.29 3.11	[44]
	UTNS	Bi_2MoO_6	300 W Xe lamp	H_2O	CO	3.62	[45]
0D/1D	QD/NW	Black P/WO_3	300 W Xenon arc lamp	H_2O	CO C_2H_4	~ 135 ~ 11	[13]
	QD (10 nm)/NT	WS_2/Bi_2S_3	300 W Xe arc lamp	H_2O	CH_3OH C_2H_5OH	9.55 6.95	[46]
	QD (3.5 nm)/NW	Ti_3C_2/Cu_2O	300 W Xe lamp	H_2O	CH_3OH	78.50	[47]
0D/2D	QD (1.6 nm)/NS	CuO/WO_3	300 W Xe lamp $\lambda > 400$ nm	H_2O	CO	1.58	[48]
	ND (4.4 nm)/NS	CND/p-CN	Xe arc lamp	H_2O	CO CH_4	5.88 2.92	[49]
	QD/NS	TiO_2/g-C_3N_4	300 W Xe lamp $\lambda > 400$ nm	MeCN/TEOA	CO	77.8	[50]
	QD (5nm)/NS	Au/TiO_2	300 W Xe arc lamp	H_2O	CO CH_4	19.75 70.34	[51]

Dimensionality	Morphology	Photocatalyst	Light Source	Reducing Agent	Main Product	Activity [$\mu mol \cdot g^{-1} \cdot h^{-1}$]	Ref.
	QD (7nm) /NS	$CsPbBr_3/Bi_2WO_6$	300 W Xe lamp λ > 400 nm	H_2O	CO/CH_4	503 $\mu mol \cdot g^{-1}$	[52]
1D/2D	NF/NS	TiO_2/MoS_2	350 W Xe lamp	H_2O	CH_4 CH_3OH	2.86 2.55	[53]
1D/2D	NT/NS	CNT/g-C_3N_4	200 W Hg and solar simulator	H_2O	CO CH_4	410 74	[54]
1D/2D	NR/NS/NF	Au/TiO_2/$BiVO_4$	300 W Xe lamp	H_2O	CO CH4	2.5 7.5	[55]
2D/2D	NS/NS	Ti_3C_2/Bi_2WO_6	300 W Xe lamp	H_2O	CH_4 CH_3OH	1.78 0.44	[56]
2D/2D	NS/NS	Bi_2WO_6/BiOI	500 W Xe arc lamp λ < 400 nm	H_2O	CH_4	2.92	[57]
2D/2D	NS/NS	Mt/m-CN	35 W Xenon lamp	H_2O/H_2	CO CH_4	505 330	[58]
2D/2D	NS/NS	SnS_2/TiO_2	300 W Xe lamp	H_2O	CH_4	23	[59]
2D/2D	NS/NS [51]	2 g-C_3N_4/$BiVO_4$	300 W Xe lamp λ ≥420 nm	H_2O	CO CH_4	5.19 4.57	[60]
2D/2D	NS/NS	PGCN/$Bi_{12}O_{17}Cl_2$	300 W xenon lamp	H_2O	CH_4	24.4	[61]
2D/2D	NP-NS/NS	Pd-g-C_3N_4 /RGOA	300 W Xe lamp	H_2O	CH_4	6.4	[62]

ation of
through
erials or
available
e stable
eering of
pecially,
y-Read-
Hall recombination).

The formation of junctions implies the presence of an internal electric field in the nanomaterial. This internal electric field can contribute to enhanced carrier behaviors such as carrier separation and transfer for the photo-induced charge carriers and to, in the end, the performance of light-driven CO_2 conversion. The internal electric field can be induced by growth of a low-dimensional semiconductor on a low-dimensional semiconductor [23][63]. The combination of two or multiple low-dimensional materials could integrate the advantages of both single units and mitigate the shortcomings of single unit by the synergistic effect [64].

One of the advantages of semiconductor QDs is the quantum size effect which is responsible for the optical properties of the photocatalyst. Apart from the acceleration of charge separation and transfer process, the contact between 0D semiconductor and 1D semiconductor provides the nanocomposite with an additional properties such as excessive electroactive sites, high surface area, and homogenous dispersion [65]. 1D Bi_2S_3 nanotubes have outstanding ability to absorb visible and near infrared light. The tubular structure of Bi_2S_3 provides the photocatalytic reaction with more active sites than other morphologies [46]. The remarkable optical and electronic properties of tungsten disulfide (WS_2) QDs can be realized due to the quantum confinement effect. WS_2 QDs can be also dispersed uniformly on the surface of Bi_2S_3 forming Bi–S channels to facilitate the charge carrier separation transfer process. The designed 0D/1D nanocomposite exhibited outstanding photocatalytic reduction of CO_2 into CH_3OH and C_2H_5OH of 38.2 $\mu mol \cdot g^{-1}$ and 27.8 $\mu mol \cdot g^{-1}$ after 4 h radiation, respectively. The improved photoreduction performance is related to the following features. Firstly, the 0D/1D nanocomposite provided combined optical and electrical properties of both WS_2 QDs and Bi_2S_3 nanotubes causing high visible and near infrared light absorption. Secondly, the enlarged surface area of the nanocomposite provided more active adsorptions site for CO_2. Thirdly, the low resistive QDs–NTs interface due to the Bi–S bonds plays a critical role for accelerated charge carrier separation [46]. $CsPbBr_3$ is widely used in the photocatalytic reactions but it suffers from the high rate of recombination during the interface transfer due to the strong reductive ability of electrons [52]. Hence, the suppression of undesired electron loss throughout the transfer process at the interface is critical factor for efficient utilization of $CsPbBr_3$. Li et al. fabricated 0D/2D nanocomposite of $CsPbBr_3/Bi_2WO_6$ via ultrasonic method with intimate contact at the interface to improve the charge separation and transfer. The Bi–Br bonds which is formed at the QDs–NSs interface is responsible for the strong interfacial interaction. The decoration of Bi_2WO_6 with $CsPbBr_3$ QDs could enhance the CO and CH_4 yield by factor of 9.5 over that of pristine $CsPbBr_3$ [52].

The building of 1D semiconductor materials on 2D semiconductors is an efficient strategy for efficient CO_2 conversion. Coupling of TiO_2 nanofibers with light harvesting semiconductors such as MoS_2 nanosheets is an efficient way to overcome the fast recombination of charge carriers and enhance the light absorption efficiency [53]. The electronic properties of MoS_2 nanosheets can be tuned by control of the thickness. The superior conversion activity of CO_2 into hydrocarbon species, that is, CH_4 and CH_3OH, resulted from the improved light harvesting, sufficient reactive sites for CO_2 adsorption, and the intimate 1D–2D chemical contact between MoS_2 and TiO_2 which could be favorable for facile and efficient charge separation upon photoexcitation [53]. The increase of the contact area between the two semiconductor nanomaterials is much more favorable to enhance the photocatalytic performance over the photocatalyst. In other words, constructing the 2D/2D interface is favorable for highly separated charge carriers at the interface. Wang et al. prepared 2D/2D heterojunctions by growth of ultrathin tin disulfide (SnS_2) onto TiO_2 nanosheets via a hydrothermal method [59]. The production yield of CH_4 over SnS_2/TiO_2 was much higher than that of pristine SnS_2 and TiO_2 nanosheets. The reason for such outstanding performance originates from the increment of the contract area between SnS_2 and TiO_2 nanosheets [59].

The photocatalytic systems with multiple junctions, that is, with multiple interfaces, displays excellent photocatalytic activity toward solar fuels generation compared to one with/without single junction [55][66][67]. Recently, Macyk and coworkers designed two heterointerface-based photocatalyst, $TiO_2/C_3N_4/Ti_3C_2$, via the interfacial assembly of Ti_3C_2 QDs on the TiO_2/C_3N_4 binary nanocomposite to boost the charge separation and transfer and providing strong redox ability in CO_2 photoreduction reaction [67]. The as-synthesized composite exhibited enhanced light absorption, suppressed electron-hole recombination, and demonstrated stable photocurrent sensitivity. The fabricated composite could overcome the disadvantage of TiO_2/C_3N_4 nanocomposites with a single junction by providing more efficient transport channels of electrons-hole pairs due to the strong interaction between Ti_3C_2 QDs and TiO_2/C_3N_4 NS. Theoretical studies demonstrated that construction of two interfacial electric fields between TiO_2/C_3N_4 and Ti_3C_2/C_3N_4 is due to electron transfer processes at the two interfaces. The interfacial built-in electric fields can promote the charge carrier separation and the photocatalytic reduction of CO_2 into CO and CH_4. Tonda et al. fabricated another multijunction system with a Bi_2WO_3/RGO/g-C_3N_4 2D/2D/2D architecture using two-step hydrothermal method for utilization in CO_2 and water reduction into useful fuels [66]. This ternary heterojunction exhibited highly improved characteristics in light harvesting ability, CO_2 adsorption capacity, photocurrent responses, and interfacial contact area. The photoconversion performance of CO_2 over Bi_2WO_3/RGO/g-C_3N_4 was dramatically enhanced toward CH_4 and CO evolution. The performance of Bi_2WO_3/RGO/g-C_3N_4 was 2.5 times higher and 3.8 times higher than those of Bi_2WO_3/RGO and RGO/g-C_3N_4, respectively [66].

3.2. Modification of Low-Dimensional Nanomaterials

Modification of nanostructured low-dimensional photocatalysts themselves are another beneficial strategy for the enhancement of photocatalytic CO_2 conversion because it helps the properties of photocatalysts to be engineered. The modification can be achieved using several approaches such as introduction of surface oxygen vacancies or the formation of a porous structure.

The efficient utilization of the solar spectrum can be controlled by tuning the band structure of the semiconductor using the elemental doping [19]. Yu et al. synthesized oxygen-doped g-C_3N_4 nanotubes via exfoliation and a 3D g-C_3N_4 curling condensation method [68]. It was found that the synthesized photocatalyst consisted of curled nanosheets that had a uniform tubular structure with 20–30 nm of diameter. The oxygen atoms can substitute for the C or N atoms in g-C_3N_4 under high temperature oxidation conditions. The oxygen doping of 1D g-C_3N_4 helped the conduction band to be at a more positive potential causing a narrower band gap and efficient light harvesting. This structure exhibited a significant methanol evolution rate of 0.88 $\mu mol \cdot g^{-1} \cdot h^{-1}$ under visible light radiation. Wu et al. synthesized self-doped black TiO_2 nanotubes arrays using a one-step aluminothermic reduction for solar-driven conversion of CO_2 into CO [69]. It is found that the average diameter of the nanotubes was 75–85 nm with 5–7 nm of wall thickness. The oxygen vacancies can act as active sites for CO_2 molecules for efficient photogenerated charge carrier separation. The visible light absorption of black TiO_2 was largely enhanced by virtue of the oxygen vacancies. The resulted photocatalytic conversion was 185.39 $\mu mol \cdot g^{-1} \cdot h^{-1}$ of CO evolution rate under visible light.

The introduction of defects into semiconductors can improve the photocatalytic activity of CO_2 into solar fuels ascribed to the promotion of photogenerated charge carrier separation and the extended light absorption [70]. Liu and coworkers prepared $Bi_{12}O_{17}Cl_2$ nanotubes with surface oxygen defects via solvothermal method [40]. The tubular structure plays crucial role for accelerating the photogenerated charge carrier separation, while the oxygen defects on the surface act as active centers for CO_2 activation. It is found that the absorption of

$Bi_{12}O_{17}Cl_2$ nanotubes is improved in the visible region compared to its bulk counterpart. The defective ultrathin tubular structure of $Bi_{12}O_{17}Cl_2$ provides effective CO_2 conversion into CO with production yield of 16.8 times higher than bulk $Bi_{12}O_{17}Cl_2$. The higher photocatalytic conversion rate can be attributed to faster charge separation on the surface of $Bi_{12}O_{17}Cl_2$ nanotubes.

The porosity of nanostructured semiconductors provides an additional feature to increase the surface area of photocatalysts, and subsequently is favorable for the solar-driven reduction of CO_2 into valuable fuels [71]. Huang et al. used a template-free method to prepare porous g-C_3N_4 with increased surface area [72]. It is reported that the porous g-C_3N_4 nanotubes had excellent photocatalytic conversion of CO_2 into CO of 40 μmol·g^{-1} within 4 h illumination. The CO yield was higher than that of bulk g-C_3N_4 by a factor of 5.6 originated from the higher surface area of the porous tubular structure, and the improved charge carrier separation and transfer process.

References

1. Halmann, M. Photoelectrochemical reduction of aqueous carbon dioxide on p-type gallium phosphide in liquid junction solar cells. Nature 1978, 275, 115–116.
2. Hemminger, J.; Carr, R.; Somorjai, G. The photoassisted reaction of gaseous water and carbon dioxide adsorbed on the SrTiO3 (111) crystal face to form methane. Chem. Phys. Lett. 1978, 57, 100–104.
3. Inoue, T.; Fujishima, A.; Konishi, S.; Honda, K. Photoelectrocatalytic reduction of carbon dioxide in aqueous suspensions of semiconductor powders. Nature 1979, 277, 637–638.
4. Zeng, S.; Kar, P.; Thakur, U.K.; Shankar, K. A review on photocatalytic CO2 reduction using perovskite oxide nanomaterials. Nanotechnology 2018, 29, 052001.
5. Zhou, B.; Song, J.; Xie, C.; Chen, C.; Qian, Q.; Han, B. Mo–Bi–Cd Ternary Metal Chalcogenides: Highly Efficient Photocatalyst for CO2 Reduction to Formic Acid Under Visible Light. ACS Sustain. Chem. Eng. 2018, 6, 5754–5759.
6. Bie, C.; Zhu, B.; Xu, F.; Zhang, L.; Yu, J. In situ grown monolayer N-doped graphene on CdS hollow spheres with seamless contact for photocatalytic CO2 reduction. Adv. Mater. 2019, 31, 1902868.
7. Billo, T.; Shown, I.; Kumar Anbalagan, A.; Effendi, T.A.; Sabbah, A.; Fu, F.-Y.; Chu, C.-M.; Woon, W.-Y.; Chen, R.-S.; Lee, C.-H. A mechanistic study of molecular CO2 interaction and adsorption on carbon implanted SnS2 thin film for photocatalytic CO2 reduction activity. Nano Energy 2020, 72, 104717.
8. Li, D.; Kassymova, M.; Cai, X.; Zang, S.-Q.; Jiang, H.-L. Photocatalytic CO2 reduction over metal-organic framework-based materials. Coord. Chem. Rev. 2020, 412, 213262.

9. Liu, W.; Li, X.; Wang, C.; Pan, H.; Liu, W.; Wang, K.; Zeng, Q.; Wang, R.; Jiang, J. A scalable general synthetic approach toward ultrathin imine-linked two-dimensional covalent organic framework nanosheets for photocatalytic CO2 reduction. J. Am. Chem. Soc. 2019, 141, 17431–17440.
10. Yang, C.; Huang, W.; da Silva, L.C.; Zhang, K.A.; Wang, X. Functional conjugated polymers for CO2 reduction using visible light. Chem. Eur. J. 2018, 24, 17454–17458.
11. Yan, Y.; Chen, J.; Li, N.; Tian, J.; Li, K.; Jiang, J.; Liu, J.; Tian, Q.; Chen, P. Systematic bandgap engineering of graphene quantum dots and applications for photocatalytic water splitting and CO2 reduction. ACS Nano 2018, 12, 3523–3532.
12. Sun, Z.; Wang, H.; Wu, Z.; Wang, L. g-C3N4 based composite photocatalysts for photocatalytic CO2 reduction. Catal. Today 2018, 300, 160–172.
13. Gao, W.; Bai, X.; Gao, Y.; Liu, J.; He, H.; Yang, Y.; Han, Q.; Wang, X.; Wu, X.; Wang, J. Anchoring of black phosphorus quantum dots onto WO3 nanowires to boost photocatalytic CO2 conversion into solar fuels. Chem. Comm. 2020, 56, 7777–7780.
14. Ren, X.; Gao, M.; Zhang, Y.; Zhang, Z.; Cao, X.; Wang, B.; Wang, X. Photocatalytic reduction of CO2 on BiOX: Effect of halogen element type and surface oxygen vacancy mediated mechanism. Appl. Catal. B 2020, 274, 119063.
15. Wang, H.; Zhang, L.; Wang, K.; Sun, X.; Wang, W. Enhanced photocatalytic CO2 reduction to methane over WO3· 0.33 H2O via Mo doping. Appl. Catal. B 2019, 243, 771–779.
16. Gao, M.; Yang, J.; Sun, T.; Zhang, Z.; Zhang, D.; Huang, H.; Lin, H.; Fang, Y.; Wang, X. Persian buttercup-like BiOBrxCl1-x solid solution for photocatalytic overall CO2 reduction to CO and O2. Appl. Catal. B 2019, 243, 734–740.
17. Samanta, S.; Yadav, R.; Kumar, A.; Sinha, A.K.; Srivastava, R. Surface modified C, O co-doped polymeric g-C3N4 as an efficient photocatalyst for visible light assisted CO2 reduction and H2O2 production. Appl. Catal. B 2019, 259, 118054.
18. Shi, R.; Chen, Y. Controlled formation of defective shell on TiO2 (001) facets for enhanced photocatalytic CO2 reduction. ChemCatChem 2019, 11, 2270–2276.
19. Tu, W.; Zhou, Y.; Zou, Z. Photocatalytic conversion of CO2 into renewable hydrocarbon fuels: State-of-the-art accomplishment, challenges, and prospects. Adv. Mater. 2014, 26, 4607–4626.
20. Razzaq, A.; In, S.-I. TiO2 based nanostructures for photocatalytic CO2 conversion to valuable chemicals. Micromachines 2019, 10, 326.
21. Huang, C.-Y.; Guo, R.-T.; Pan, W.-G.; Tang, J.-Y.; Zhou, W.-G.; Liu, X.-Y.; Qin, H.; Jia, P.-Y. One-dimension TiO2 nanostructures with enhanced activity for CO2 photocatalytic reduction. Appl. Surf. Sci. 2019, 464, 534–543.

22. Patil, S.B.; Basavarajappa, P.S.; Ganganagappa, N.; Jyothi, M.; Raghu, A.; Reddy, K.R. Recent advances in non-metals-doped TiO2 nanostructured photocatalysts for visible-light driven hydrogen production, CO2 reduction and air purification. Int. J. Hydrog. Energy 2019, 44, 13022–13039.
23. Xu, H.-M.; Wang, H.-C.; Shen, Y.; Lin, Y.-H.; Nan, C.-W. Low-dimensional nanostructured photocatalysts. J. Adv. Ceram. 2015, 4, 159–182.
24. Chang, X.; Wang, T.; Gong, J. CO2 photo-reduction: Insights into CO2 activation and reaction on surfaces of photocatalysts. Energy Environ. Sci. 2016, 9, 2177–2196.
25. Mao, J.; Li, K.; Peng, T. Recent advances in the photocatalytic CO2 reduction over semiconductors. Catal. Sci. Technol. 2013, 3, 2481–2498.
26. Markovits, A.; Fahmi, A.; Minot, C. A theoretical study of CO2 adsorption on TiO2. J. Mol. Struct. THEOCHEM 1996, 371, 219–235.
27. Sharma, N.; Das, T.; Kumar, S.; Bhosale, R.; Kabir, M.; Ogale, S. Photocatalytic activation and reduction of CO2 to CH4 over single phase nano Cu3SnS4: A combined experimental and theoretical study. ACS Appl. Energy Mater. 2019, 2, 5677–5685.
28. Indrakanti, V.P.; Kubicki, J.D.; Schobert, H.H. Photoinduced activation of CO2 on Ti-based heterogeneous catalysts: Current state, chemical physics-based insights and outlook. Energy Environ. Sci. 2009, 2, 745–758.
29. Álvarez, A.; Borges, M.; Corral-Pérez, J.J.; Olcina, J.G.; Hu, L.; Cornu, D.; Huang, R.; Stoian, D.; Urakawa, A. CO2 activation over catalytic surfaces. ChemPhysChem 2017, 18, 3135–3141.
30. Fu, J.; Jiang, K.; Qiu, X.; Yu, J.; Liu, M. Product selectivity of photocatalytic CO2 reduction reactions. Mater. Today 2020, 32, 222–243.
31. Khan, A.A.; Tahir, M. Recent advancements in engineering approach towards design of photo-reactors for selective photocatalytic CO2 reduction to renewable fuels. J. CO2 Util. 2019, 29, 205–239.
32. Linsebigler, A.L.; Lu, G.; Yates, J.T., Jr. Photocatalysis on TiO2 surfaces: Principles, mechanisms, and selected results. Chem. Rev. 1995, 95, 735–758.
33. Hou, J.; Cao, S.; Wu, Y.; Gao, Z.; Liang, F.; Sun, Y.; Lin, Z.; Sun, L. Inorganic colloidal perovskite quantum dots for robust solar CO2 reduction. Chem. Eur. J. 2017, 23, 9481–9485.
34. Sheng, J.; He, Y.; Li, J.; Yuan, C.; Huang, H.; Wang, S.; Sun, Y.; Wang, Z.; Dong, F. Identification of halogen-associated active sites on bismuth-based perovskite quantum dots for efficient and selective CO2-to-CO photoreduction. ACS Nano 2020, 14, 13103–13114.
35. Zhou, L.; Xu, Y.F.; Chen, B.X.; Kuang, D.B.; Su, C.Y. Synthesis and Photocatalytic Application of Stable Lead-Free Cs2AgBiBr6 Perovskite Nanocrystals. Small 2018, 14, 1703762.

36. Que, M.; Zhao, Y.; Pan, L.; Yang, Y.; He, Z.; Yuan, H.; Chen, J.; Zhu, G. Colloidal formamidinium lead bromide quantum dots for photocatalytic CO2 reduction. Mater. Lett. 2021, 282, 128695.

37. Zhu, C.; Wei, X.; Li, W.; Pu, Y.; Sun, J.; Tang, K.; Wan, H.; Ge, C.; Zou, W.; Dong, L. Crystal-Plane Effects of CeO2 and CeO2 on Photocatalytic CO2 Reduction: Synergistic Interactions of Oxygen Defects and Hydroxyl Groups. ACS Sustain. Chem. Eng. 2020, 8, 14397–14406.

38. Liu, B.; Ye, L.; Wang, R.; Yang, J.; Zhang, Y.; Guan, R.; Tian, L.; Chen, X. Phosphorus-doped graphitic carbon nitride nanotubes with amino-rich surface for efficient CO2 capture, enhanced photocatalytic activity, and product selectivity. ACS Appl. Mater. Interfaces 2018, 10, 4001–4009.

39. Mo, Z.; Zhu, X.; Jiang, Z.; Song, Y.; Liu, D.; Li, H.; Yang, X.; She, Y.; Lei, Y.; Yuan, S. Porous nitrogen-rich g-C3N4 nanotubes for efficient photocatalytic CO2 reduction. Appl. Catal. B 2019, 256, 117854.

40. Di, J.; Zhu, C.; Ji, M.; Duan, M.; Long, R.; Yan, C.; Gu, K.; Xiong, J.; She, Y.; Xia, J. Defect-Rich Bi12O17Cl2 Nanotubes Self-Accelerating Charge Separation for Boosting Photocatalytic CO2 Reduction. Angew. Chem. Int. Ed. 2018, 57, 14847–14851.

41. Di, J.; Song, P.; Zhu, C.; Chen, C.; Xiong, J.; Duan, M.; Long, R.; Zhou, W.; Xu, M.; Kang, L. Strain-Engineering of Bi12O17Br2 Nanotubes for Boosting Photocatalytic CO2 Reduction. ACS Mater. Lett. 2020, 2, 1025–1032.

42. Xu, G.; Zhang, H.; Wei, J.; Zhang, H.-X.; Wu, X.; Li, Y.; Li, C.; Zhang, J.; Ye, J. Integrating the g-C3N4 Nanosheet with B–H bonding decorated metal–organic framework for CO2 activation and photoreduction. ACS Nano 2018, 12, 5333–5340.

43. Xia, P.; Zhu, B.; Yu, J.; Cao, S.; Jaroniec, M. Ultra-thin nanosheet assemblies of graphitic carbon nitride for enhanced photocatalytic CO2 reduction. J. Mater. Chem. A 2017, 5, 3230–3238.

44. Han, C.; Wang, B.; Wu, C.; Shen, S.; Zhang, X.; Sun, L.; Tian, Q.; Lei, Y.; Wang, Y. Ultrathin SiC nanosheets with high reduction potential for improved CH4 generation from photocatalytic reduction of CO2. ChemistrySelect 2019, 4, 2211–2217.

45. Di, J.; Zhao, X.; Lian, C.; Ji, M.; Xia, J.; Xiong, J.; Zhou, W.; Cao, X.; She, Y.; Liu, H. Atomically-thin Bi2MoO6 nanosheets with vacancy pairs for improved photocatalytic CO2 reduction. Nano Energy 2019, 61, 54–59.

46. Dai, W.; Yu, J.; Luo, S.; Hu, X.; Yang, L.; Zhang, S.; Li, B.; Luo, X.; Zou, J. WS2 quantum dots seeding in Bi2S3 nanotubes: A novel Vis-NIR light sensitive photocatalyst with low-resistance junction interface for CO2 reduction. Chem. Eng. J. 2020, 389, 123430.

47. Zeng, Z.; Yan, Y.; Chen, J.; Zan, P.; Tian, Q.; Chen, P. Boosting the photocatalytic ability of Cu2O nanowires for CO2 conversion by MXene quantum dots. Adv. Funct. Mater. 2019, 29, 1806500.

48. Xie, Z.; Xu, Y.; Li, D.; Chen, L.; Meng, S.; Jiang, D.; Chen, M. Construction of CuO quantum Dots/WO3 nanosheets 0D/2D Z-scheme heterojunction with enhanced photocatalytic CO2 reduction activity under visible-light. J. Alloys Compd. 2021, 858, 157668.
49. Ong, W.-J.; Putri, L.K.; Tan, Y.-C.; Tan, L.-L.; Li, N.; Ng, Y.H.; Wen, X.; Chai, S.-P. Unravelling charge carrier dynamics in protonated g-C3N4 interfaced with carbon nanodots as co-catalysts toward enhanced photocatalytic CO2 reduction: A combined experimental and first-principles DFT study. Nano Res. 2017, 10, 1673–1696.
50. Shi, H.; Long, S.; Hu, S.; Hou, J.; Ni, W.; Song, C.; Li, K.; Gurzadyan, G.G.; Guo, X. Interfacial charge transfer in 0D/2D defect-rich heterostructures for efficient solar-driven CO2 reduction. Appl. Catal. B 2019, 245, 760–769.
51. Wang, R.; Shen, J.; Sun, K.; Tang, H.; Liu, Q. Enhancement in photocatalytic activity of CO2 reduction to CH4 by 0D/2D Au/TiO2 plasmon heterojunction. Appl. Surf. Sci. 2019, 493, 1142–1149.
52. Wang, J.; Wang, J.; Li, N.; Du, X.; Ma, J.; He, C.; Li, Z. Direct Z-Scheme 0D/2D Heterojunction of CsPbBr3 Quantum Dots/Bi2WO6 Nanosheets for Efficient Photocatalytic CO2 Reduction. ACS Appl. Mater. Interfaces 2020, 12, 31477–31485.
53. Xu, F.; Zhu, B.; Cheng, B.; Yu, J.; Xu, J. 1D/2D TiO2/MoS2 hybrid nanostructures for enhanced photocatalytic CO2 reduction. Adv. Opt. Mater. 2018, 6, 1800911.
54. Tahir, M.; Tahir, B.; Nawawi, M.; Hussain, M.; Muhammad, A. Cu-NPs embedded 1D/2D CNTs/pCN heterojunction composite towards enhanced and continuous photocatalytic CO2 reduction to fuels. Appl. Surf. Sci. 2019, 485, 450–461.
55. Bian, J.; Qu, Y.; Zhang, X.; Sun, N.; Tang, D.; Jing, L. Dimension-matched plasmonic Au/TiO2/BiVO4 nanocomposites as efficient wide-visible-light photocatalysts to convert CO2 and mechanistic insights. J. Mater. Chem. A 2018, 6, 11838–11845.
56. Cao, S.; Shen, B.; Tong, T.; Fu, J.; Yu, J. 2D/2D heterojunction of ultrathin MXene/Bi2WO6 nanosheets for improved photocatalytic CO2 reduction. Adv. Funct. Mater. 2018, 28, 1800136.
57. Kong, X.Y.; Lee, W.Q.; Mohamed, A.R.; Chai, S.-P. Effective steering of charge flow through synergistic inducing oxygen vacancy defects and pn heterojunctions in 2D/2D surface-engineered Bi2WO6/BiOI cascade: Towards superior photocatalytic CO2 reduction activity. Chem. Eng. J. 2019, 372, 1183–1193.
58. Tahir, B.; Tahir, M.; Yunus, M.A.C.; Mohamed, A.R.; Siraj, M.; Fatehmulla, A. 2D/2D Mt/m-CN composite with enriched interface charge transfer for boosting photocatalytic CO2 hydrogenation by H2 to CH4 under visible light. Appl. Surf. Sci. 2020, 520, 146296.
59. She, H.; Zhou, H.; Li, L.; Zhao, Z.; Jiang, M.; Huang, J.; Wang, L.; Wang, Q. Construction of a two-dimensional composite derived from TiO2 and SnS2 for enhanced photocatalytic reduction of

CO2 into CH4. ACS Sustain. Chem. Eng. 2018, 7, 650–659.

60. Lu, M.; Li, Q.; Zhang, C.; Fan, X.; Li, L.; Dong, Y.; Chen, G.; Shi, H. Remarkable photocatalytic activity enhancement of CO2 conversion over 2D/2D g-C3N4/BiVO4 Z-scheme heterojunction promoted by efficient interfacial charge transfer. Carbon 2020, 160, 342–352.
61. Huo, Y.; Zhang, J.; Wang, Z.; Dai, K.; Pan, C.; Liang, C. Efficient interfacial charge transfer of 2D/2D porous carbon nitride/bismuth oxychloride step-scheme heterojunction for boosted solar-driven CO2 reduction. J. Colloid Interface Sci. 2021, 585, 684–693.
62. Zhang, R.; Huang, Z.; Li, C.; Zuo, Y.; Zhou, Y. Monolithic g-C3N4/reduced graphene oxide aerogel with in situ embedding of Pd nanoparticles for hydrogenation of CO2 to CH4. Appl. Surf. Sci. 2019, 475, 953–960.
63. Akhundi, A.; Habibi-Yangjeh, A.; Abitorabi, M.; Rahim Pouran, S. Review on photocatalytic conversion of carbon dioxide to value-added compounds and renewable fuels by graphitic carbon nitride-based photocatalysts. Catal. Rev. 2019, 61, 595–628.
64. He, Z.; Zhang, J.; Li, X.; Guan, S.; Dai, M.; Wang, S. 1D/2D Heterostructured Photocatalysts: From Design and Unique Properties to Their Environmental Applications. Small 2020, 16, 2005051.
65. Li, B.; Cao, Z.; Wang, S.; Wei, Q.; Shen, Z. BiVO4 quantum dot-decorated BiPO4 nanorods 0D/1D heterojunction for enhanced visible-light-driven photocatalysis. Dalton Trans. 2018, 47, 10288–10298.
66. Jo, W.-K.; Kumar, S.; Eslava, S.; Tonda, S. Construction of Bi2WO6/RGO/g-C3N4 2D/2D/2D hybrid Z-scheme heterojunctions with large interfacial contact area for efficient charge separation and high-performance photoreduction of CO2 and H2O into solar fuels. Appl. Catal. B 2018, 239, 586–598.
67. He, F.; Zhu, B.; Cheng, B.; Yu, J.; Ho, W.; Macyk, W. 2D/2D/0D TiO2/C3N4/Ti3C2 MXene composite S-scheme photocatalyst with enhanced CO2 reduction activity. Appl. Catal. B 2020, 272, 119006.
68. Fu, J.; Zhu, B.; Jiang, C.; Cheng, B.; You, W.; Yu, J. Hierarchical porous O-doped g-C3N4 with enhanced photocatalytic CO2 reduction activity. Small 2017, 13, 1603938.
69. Gao, J.; Shen, Q.; Guan, R.; Xue, J.; Liu, X.; Jia, H.; Li, Q.; Wu, Y. Oxygen vacancy self-doped black TiO2 nanotube arrays by aluminothermic reduction for photocatalytic CO2 reduction under visible light illumination. J. CO2 Util. 2020, 35, 205–215.
70. Xiu, Z.; Guo, M.; Zhao, T.; Pan, K.; Xing, Z.; Li, Z.; Zhou, W. Recent advances in Ti3+ self-doped nanostructured TiO2 visible light photocatalysts for environmental and energy applications. Chem. Eng. J. 2020, 382, 123011.

71. Wang, H.; Liu, X.; Niu, P.; Wang, S.; Shi, J.; Li, L. Porous two-dimensional materials for photocatalytic and electrocatalytic applications. Matter 2020, 2, 1377–1413.
72. Tian, N.; Xiao, K.; Zhang, Y.; Lu, X.; Ye, L.; Gao, P.; Ma, T.; Huang, H. Reactive sites rich porous tubular yolk-shell g-C3N4 via precursor recrystallization mediated microstructure engineering for photoreduction. Appl. Catal. B 2019, 253, 196–205.